# On the Photo-thermal Effect of Intra-body Nano-optical Communications on Red Blood Cells

Shuanshuan Wu, Pedram Johari, Nicholas Mastronarde, and Josep Miquel Jornet
Department of Electrical Engineering, University at Buffalo, Buffalo, New York 14260
Email: {shuanshu, pedramjo, nmastron, jmjornet}@buffalo.edu

***Abstract*—In the near future, it is envisioned that intra-body nanosensing systems will provide fast and accurate disease diagnosis and treatment. Recent work on intra-body communications has focused on understanding the propagation of electromagnetic (EM) signals in biological media; however, the photo-thermal effects of the EM waves on biological tissues are not as well understood, despite the risk of damaging the tissues. In this paper, we consider an intra-body nanosensing system where active nanoparticles (NPs) are injected into blood vessels. Using stochastic geometry, we analytically model the photo-thermal effect on red blood cells (RBCs) induced by EM waves of NP transmissions. Numerical results validate the proposed analytical model and provide insights into the safety of such systems.**

## I. Introduction

Novel nanosensors enabled by nanotechnologies are able to detect various types of events at the nanoscale with unprecedented accuracy. Intra-body nanosensing systems, which operate inside the human body in real time, have been proposed to provide fast and accurate diagnosis and treatment of diverse diseases ranging from neuronal disorders [1] to different types of cancer [2], all directly from blood. In such systems, biocompatible nanosensors injected or implanted in the human body are configured to transmit the sensed information to a common sink, receive commands from a remote controller, or coordinate joint actions when needed [3].

In many of such intra-body nanosensing systems, nanoparticles (NPs) radiate electromagnetic (EM) waves, either passively (e.g., gold NPs) or actively (e.g., injected nanomachines). As a result, molecules that are present in the medium are excited by EM waves. An excited molecule internally vibrates, i.e., its atoms show periodic motion while the molecule as a whole has constant translational and rotational motions. As a result, part of the energy of the propagating wave is converted to kinetic energy [4]. From the communications perspective, such conversion results in signal loss. On the other hand, vibrating molecules can induce increase in the cells temperature, as "trapped" molecules trying to vibrate suffer from friction. The temperature increase may be harmful to healthy biological cells based on their photo-thermal sensitivity.

Intuitively, the temperature increase of a biological cell depends on the density of NPs that are radiating EM waves and the time that the cell is exposed to the EM waves. More heat may be generated at a cell when there are more NPs nearby. Additionally, longer radiating times of NPs means more accumulated kinetic energy at the cell. Cumulative Equivalent Minutes at 43 °C ($\text{CEM}_{43}$) is the accepted metric for thermal exposure (temperature and time of exposure) that correlates well with thermal damage in a variety of tissues [5]. Therefore, before injecting/implanting NPs into the human body, it is important to quantitatively understand these effects so that they can be predicted and controlled, and potential tissue damage can be avoided.

This can be done using simulations, with specific tissue compositions and NP configurations. In [6], based on deterministic models, the authors analyzed the heating effects due to single as well as multiple NPs radiating EM waves, and simulated a case study of the temperature increase in red blood cells by means of COMSOL simulations [7]. Alternatively, this can be done analytically based on stochastic models. The latter choice is attractive: if we can develop a tractable analytical framework to model the problem, then the temperature increase in human tissues can be quickly determined under various parameter configurations.

Assuming that the spatial distributions of biological cells and NPs can be modeled as point processes [8], it is possible to analyze the intra-body nanosensing system using stochastic geometry [9]. Stochastic geometry has already played an important role in modeling wireless networks, e.g., analyzing the distribution of interference and the signal-to-interference-plus-noise ratio (SINR) in cellular networks [10].

In this paper, we stochastically model the temperature increase of a cell (induced by EM radiation from NPs) assuming that cells and NPs are distributed according to Poisson Point Processes (PPPs) within their surrounding biological medium. Specifically, we consider the temperature increase of RBCs induced by EM radiation from active NPs injected into the blood vessels. We assume that the NPs operate at visible optical frequencies 400–700 THz, which is the case for the majority of NP-based nano-biosensing systems. The main reason for this is the relatively small absorption loss at visible optical frequencies in biological tissues, which are mostly water (by volume, up to $95\%$ of blood plasma is water).

This paper makes the following contributions.

- We derive the line-of-sight (LOS) probability between an NP and a typical RBC so we can model the intensity of incident EM waves at the RBC.
- We derive the Laplace transform, expectation, and variance of the temperature increase at a typical RBC.
- Using the Laplace transform and LOS probability, we derive an approximate closed-form expression for the distribution of the temperature increase of the RBCs.

978-1-5386-5979-3/18/$31.00 ©2018 IEEE

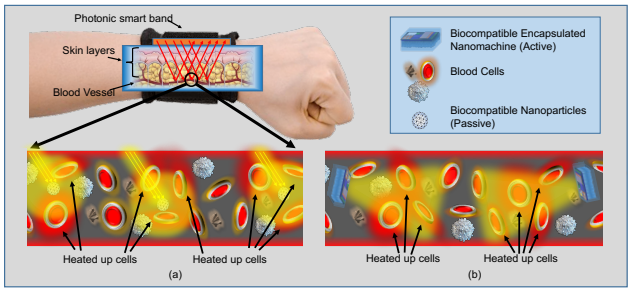


Fig. 1: System model for intra-body EM communications (a) with passive reflecting nanoparticles and (b) with active nanomachines.

- We validate our models against numerical results.

The above contributions help us quantitatively and analytically understand the temperature increase of RBCs induced by EM waves from active NPs, so that the operation of intra-body optical wireless communications can be performed without damaging RBCs. Note that the analysis can be modified to consider the passive NP case by accounting for the contribution of the background EM field (that is used to excite the NPs) to the photo-thermal effect.

The remainder of the paper is organized as follows. In Sec. II, we present the system model. In Sec. III, we analyze the temperature increase of RBCs. In Sec. IV, we present numerical results to validate the analytical models and provide insights on nanosensing system design. We conclude in Sec. V.

## II. Intra-body Nanosensing System Model

We consider an intra-body nanosensing system in which NPs are injected into blood vessels. Fig. 1 shows two examples of NPs that operate in blood vessels: passive NPs [Fig. 1(a)] and active NPs [Fig. 1(b)]. The latter are also referred to as nanomachines. In passive NP operation, the system uses passive reflecting NPs that are excited by an external source; while in active NP operation, NPs are equipped with nano-antennas that can radiate EM waves by themselves. With bio-compatible NPs injected into the blood stream, we study the temperature increase of blood cells induced by EM waves. Blood is composed of living cells (red blood cells [RBCs] and white blood cells [WBCs]) and non-living matrix, i.e., blood plasma. Here we ignore WBCs since WBCs comprise less than $1\%$ of blood by volume, and some WBCs are transparent, i.e., they have similar optical properties as that of plasma [17]. As a result, the blood is assumed to be composed of RBCs immersed in homogeneous plasma and we focus our analysis on the temperature increase of RBCs.

### A. Geometric Assumptions

We model the spatial locations of RBCs and NPs as 3D homogeneous PPPs. A PPP defined in $\mathbb{R}^3$ is a random process in which the number of points $\Phi$ in a bounded Borel set $\mathsf{B} \subset \mathbb{R}^3$ has a Poisson distribution [9]:

$$\mathbb{P}(\Phi(\mathsf{B}) = k) = \frac{\Lambda^k}{k!} e^{-\Lambda}, \ k = 0, 1, 2, ... \tag{1}$$

where $\Lambda = \int_{\mathcal{B}} \lambda(\boldsymbol{x}) \mathrm{d}\boldsymbol{x}$ is the expectation of the Poisson random variable for some intensity function $\lambda(\boldsymbol{x})$. If $\lambda(\boldsymbol{x})$ is constant, i.e., $\lambda(\boldsymbol{x}) = \lambda$, the PPP is said to be homogeneous. In the remainder of the paper, let $\Phi_{\mathrm{c}}$ and $\Phi_{\mathrm{p}}$ denote the PPPs of RBCs and NPs, respectively; and $\lambda_{\mathrm{c}}$ and $\lambda_{\mathrm{p}}$ denote the corresponding intensities.

Throughout this paper, we focus our analysis on a randomly selected typical cell that, without loss of generality, we assume is located at the origin $\boldsymbol{o}$ of $\mathbb{R}^3$. This is permissible in a homogeneous PPP by Slivnyak's theorem [9].

### B. LOS Model

Due to cell absorption, the EM waves that pass through cells have very weak strength. Moreover, there is no significant diffraction/scattering since the size of the cells is much larger than the visible light wavelength, i.e., several micrometers (μm) vs. hundreds of nanometers (nm). As a result, the heat generated by blocked NPs may be very weak and we focus only on the heat induced by LOS EM waves.[1] It is noted that obstacles that block the LOS path can be either RBCs or NPs.

We derive the LOS probability expression between a randomly picked NP and the typical RBC separated by distance $d$. Since an obstacle can be either another RBC or another NP, the obstacle point process is the superposition of point processes of the RBCs and NPs, i.e., obstacles can still be modeled as a homogeneous PPP with intensity $\lambda_{\mathrm{o}} = \lambda_{\mathrm{c}} + \lambda_{\mathrm{p}}$. For the LOS probability model, we assume that each obstacle $o_i$ has independent radius $r_{o_i}$ with probability density function (PDF) $f_{r_o}(x)$ defined in $[r_o^{\min}, r_o^{\max}]$. The derivation of the LOS probability is similar to [14], but extended to 3D PPPs. We thus omit the derivation but present the conclusion as follows.

**Lemma 1.** The LOS probability between an NP and an RBC with distance $d$ is $p_{\mathrm{L}}(d) = c_1 e^{-c_2 d}$, where $c_1 = \exp\left(-\frac{4}{3}\pi\lambda_{\mathrm{o}}\mathbb{E}[r_o^3]\right)$ and $c_2 = \pi\lambda_{\mathrm{o}}\mathbb{E}[r_o^2]$. ■

### C. Antenna Propagation Pattern Models

Antenna model of NPs can be either omni-directional or directional. An omni-directional antenna pattern has uniform antenna gain over all directions and a directional antenna has the ability to concentrate the radiated power in a specific direction. For tractability, we consider a cone radiation pattern with main lobe approximated by a right circular cone. The antenna gain is denoted by $\mathcal{G}$. Under our directional cone antenna model, we assume that the antenna boresight of a randomly selected NP is uniformly distributed over $360° \times 360°$. It is easy to verify that the antenna gain of a random NP is

$$\mathcal{G} = \begin{cases} g_{\mathrm{mn}}, & \text{with probability } \frac{1-\cos\psi}{2} \triangleq a_{\mathrm{mn}} \\ g_{\mathrm{sd}}, & \text{with probability } \frac{1+\cos\psi}{2} \triangleq a_{\mathrm{sd}}, \end{cases} \tag{2}$$

where $g_{\mathrm{mn}}$ and $g_{\mathrm{sd}}$ are the main and side lobe antenna gains, respectively; and $\psi$ is half of the main lobe beam width. Fig. 2 shows an example of the directional antenna gains of a cone

[1] Recent research has revealed that some tissue cells (e.g., RBCs) actually act as lenses that focus the EM waves in a very short range after passing through a cell [11], [12], [13]. However, due to their short range, we expect that the temperature increase induced by these focused EM waves is significantly smaller than that induced by the LOS EM waves. For simplicity, we ignore the focus effect in this paper and leave it for future research.

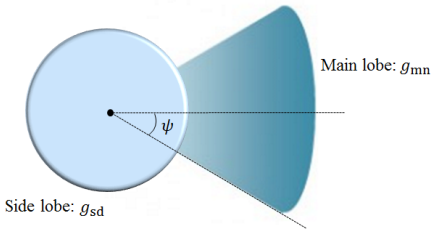


Fig. 2: Main and side lobe gains in the cone antenna model.

antenna model. Note that the main and side lobe gains satisfy the condition that $a_{\text{mn}}g_{\text{mn}} + a_{\text{sd}}g_{\text{sd}} = 1$.

### D. Temperature Increase Model

Due to the heat dissipation effect, when a cell's temperature goes higher than the medium's temperature, the heat energy accumulated at the cell starts to dissipate to the medium. As a result, the temperature change of a cell at some specific time can be modeled as

$$\Delta T_{\text{tot}} = \Delta T - \widetilde{\Delta T}, \tag{3}$$

where $\Delta T$ is the temperature increase induced by EM radiation, and $\widetilde{\Delta T}$ is the temperature decrease due to heat dissipation. In this paper, we only focus on analyzing $\Delta T$, but will model the dissipation effect in future work so that we can understand how the temperature evolves over time. Note that, we may approximate $\Delta T_{\text{tot}} \approx \Delta T$ in a very short time interval; therefore, $\Delta T$ can be considered as an upper limit on the temperature increase.

Given a typical cell with absorption cross section $\sigma_{\text{a}}$ (area), the heat power delivered by an NP $r$ away is [15]

$$q(r) = \sigma_{\text{a}} I(r), \tag{4}$$

where $I(r)$ is the irradiance of the illumination with dimension power per area (power density). The irradiance $I(r)$ is directly related to electric field with the equation $I(r) = \frac{c_{\text{m}}\epsilon_{\text{m}}}{2}|\mathbf{E}(r)|^2$, where $\mathbf{E}(r)$ is the electric field, $c_{\text{m}}$ is the wave speed in the medium, and $\epsilon_{\text{m}}$ is the absolute permittivity of the medium. When we consider the medium to be homogeneous, the irradiance of the illumination also relates to the transmission power $P_{\text{t}}$ of the NP that

$$I(r) = \mathcal{G}\frac{P_{\text{t}}}{4\pi r^2}e^{-\alpha_{\text{a}} r}, \tag{5}$$

where $\alpha_{\text{a}}$ is the absorption coefficient of the medium.

The temperature increase of the typical cell induced by the radiation of the NP is modeled as

$$\Delta T(t) = \frac{q(r)t}{\mathsf{c}_{\text{c}}\mathsf{m}_{\text{c}}} = \frac{\sigma_{\text{a}} t}{\mathsf{c}_{\text{c}}\mathsf{m}_{\text{c}}} I(r), \tag{6}$$

where $t$ is the NP's radiation time and $\mathsf{c}_{\text{c}}$ and $\mathsf{m}_{\text{c}}$ are the cell's specific heat capacity and mass, respectively.

Note that, due to their size and energy constraints, we assume that NPs transmit very short pulse signals with duration $t_{\text{on}}$ in a transmission period of duration $t_p$. Thus, the maximum temperature increase induced by a single NP in one transmission period is achieved at $t = t_{\text{on}}$, i.e., $\Delta T_{\text{max}} = \Delta T(t_{\text{on}})$.

When there are multiple NPs nearby, the total temperature increase depends on each NP's transmission timeline. If the transmission periods are aligned, e.g., the system uses passive reflecting NPs that are excited by a common external source [Fig. 1(a)], then the temperature increase is still maximized at $t = t_{\text{on}}$. However, if the NPs' transmissions are not aligned, e.g., the system uses unsychronized active nanomachines [Fig. 1(b)], then the situation is slightly different. Since inactive NPs can be removed by independent thinning according to the duty cycle $\frac{t_{\text{on}}}{t_p}$, the effective NPs still form a homogeneous PPP $\Phi_{\bar{\text{p}}}$ with intensity $\lambda_{\bar{\text{p}}} = \frac{t_{\text{on}}}{t_p}\lambda_{\text{p}}$. Given the effective NP intensity $\lambda_{\bar{\text{p}}}$, the total temperature increase in time duration $t_{\text{on}}$ is

$$\Delta T = \sum_{k\in\Phi_{\bar{\text{p}}}} \mathcal{B}_k c_3 \mathcal{G}_k \frac{e^{-\alpha_{\text{a}} r}}{r_k^2}, \tag{7}$$

where $c_3 = \frac{\sigma_{\text{a}} t_{\text{on}} P_{\text{t}}}{4\pi \mathsf{c}_{\text{c}}\mathsf{m}_{\text{c}}}$, $r_k$ is the distance from NP $k$ to the RBC, and $\mathcal{B}_k$ is a Bernoulli random variable with parameter $p_{\text{L}}(r_k)$.

## III. Temperature Increase Analysis

In this section, based on the system model introduced in Sec. II, we analytically derive the temperature increase of a typical RBC induced by EM radiation from the active NPs. Specifically, we derive the Laplace transform of $\Delta T$, i.e., $\mathcal{L}_{\Delta T}(s)$. Given $\mathcal{L}_{\Delta T}(s)$, we can gain insights into the statistical properties of $\Delta T$.

Let $r_{\text{c}}$ denote the radius of the typical cell. We have the following conclusion regarding the Laplace transform of $\Delta T$. The derivation can be found in Appendix A.

**Proposition 1.** The Laplace transform of $\Delta T$ is given as

$$\mathcal{L}_{\Delta T}(s) = E_1 e^{L_{\text{mn}}(s) + L_{\text{sd}}(s)}, \tag{8}$$

where $E_1 = \exp\left(-4\pi\lambda_{\bar{\text{p}}}c_1\frac{e^{-c_2 r_{\text{c}}}}{c_2^3}(c_2^2 r_{\text{c}}^2 + 2c_2 r_{\text{c}} + 2)\right)$, $L_{\text{mn}}(s) = 4\pi a_{\text{mn}}\lambda_{\bar{\text{p}}}c_1\int_{r>r_{\text{c}}} r^2 e^{-c_2 r} e^{-s c_{3,\text{m}} r^{-2} e^{-\alpha_{\text{a}} r}}\text{d}r$, $L_{\text{sd}}(s) = 4\pi a_{\text{sd}}\lambda_{\bar{\text{p}}}c_1\int_{r>r_{\text{c}}} r^2 e^{-c_2 r} e^{-s c_{3,\text{s}} r^{-2} e^{-\alpha_{\text{a}} r}}\text{d}r$, $c_{3,\text{m}} = c_3 g_{\text{mn}}$, and $c_{3,\text{s}} = c_3 g_{\text{sd}}$. ■

In Proposition 1, we assume that NPs are equipped with directional antennas. When omni-directional antennas are used ($\mathcal{G} = 0$ dB), the Laplace transform of $\Delta T$ is simplified to

$$\mathcal{L}_{\Delta T}(s) = E_1 \cdot e^{4\pi\lambda_{\bar{\text{p}}}c_1\int_{r>r_{\text{c}}} r^2 e^{-c_2 r}\exp\left(-s c_3 r^{-2} e^{-\alpha_{\text{a}} r}\right)\text{d}r}.$$

Moments of a random variable can be determined from its Laplace transform. Denote by $X$ a random variable with PDF $f_X(x)$. Recall that from the definition of Laplace transform, we have $\mathcal{L}_X(s) = \sum_{n=0}^{\infty}\frac{(-1)^n M_n}{n!}s^n$. The $n$th moment of $X$ can thus be determined as

$$M_n = (-1)^n \mathcal{L}_X^{(n)}(s)|_{s=0}, \tag{9}$$

where $\mathcal{L}_X^{(n)}(s)|_{s=0}$ is the $n$th order derivative of $\mathcal{L}_X(s)$ evaluated at $s = 0$. In other words, given the Laplace transform, statistical properties of a random variable can be uniquely determined.

For example, mean and variance are determined by the first and second order derivatives of $\mathcal{L}_{\Delta T}(s)$, which are derived as

$$\mathcal{L}^{(1)}_{\Delta T}(s) = -4\pi\lambda_{\bar{\mathrm{p}}}c_1\mathcal{L}_{\Delta T}(s)\times \left(a_{\mathrm{mn}}c_{3,\mathrm{m}}\int_{r>r_{\mathrm{c}}} e^{-(c_2+\alpha_{\mathrm{a}})r}\exp(-sc_{3,\mathrm{m}}r^{-2}e^{-\alpha_{\mathrm{a}}r})\mathrm{d}r + a_{\mathrm{sd}}c_{3,\mathrm{s}}\int_{r>r_{\mathrm{c}}} e^{-(c_2+\alpha_{\mathrm{a}})r}\exp(-sc_{3,\mathrm{s}}r^{-2}e^{-\alpha_{\mathrm{a}}r})\mathrm{d}r\right),$$

and

$$\begin{aligned}\mathcal{L}^{(2)}_{\Delta T}(s) = &-4\pi\lambda_{\bar{\mathrm{p}}}c_1\mathcal{L}^{(1)}_{\Delta T}(s)\times \left(a_{\mathrm{mn}}c_{3,\mathrm{m}}\int_{r>r_{\mathrm{c}}} e^{-(c_2+\alpha_{\mathrm{a}})r}\exp(-sc_{3,\mathrm{m}}r^{-2}e^{-\alpha_{\mathrm{a}}r})\mathrm{d}r + a_{\mathrm{sd}}c_{3,\mathrm{s}}\int_{r>r_{\mathrm{c}}} e^{-(c_2+\alpha_{\mathrm{a}})r}\exp(-sc_{3,\mathrm{s}}r^{-2}e^{-\alpha_{\mathrm{a}}r})\mathrm{d}r\right)\\ &+4\pi\lambda_{\bar{\mathrm{p}}}c_1\mathcal{L}_{\Delta T}(s)\times \left(a_{\mathrm{mn}}c^2_{3,\mathrm{m}}\int_{r>r_{\mathrm{c}}} r^{-2}e^{-(c_2+2\alpha_{\mathrm{a}})r}\exp(-sc_{3,\mathrm{m}}r^{-2}e^{-\alpha_{\mathrm{a}}r})\mathrm{d}r + a_{\mathrm{sd}}c^2_{3,\mathrm{s}}\int_{r>r_{\mathrm{c}}} r^{-2}e^{-(c_2+2\alpha_{\mathrm{a}})r}\exp(-sc_{3,\mathrm{s}}r^{-2}e^{-\alpha_{\mathrm{a}}r})\mathrm{d}r\right).\end{aligned}$$

It can be verified that $\mathcal{L}_{\Delta T}(s)|_{s=0} = 1$. The two derivatives evaluated at $s = 0$ are

$$\begin{aligned}&\mathcal{L}^{(1)}_{\Delta T}(s)|_{s=0}\\ &= -4\pi\lambda_{\bar{\mathrm{p}}}c_1(a_{\mathrm{mn}}c_{3,\mathrm{m}} + a_{\mathrm{sd}}c_{3,\mathrm{s}})\int_{r>r_{\mathrm{c}}} e^{-(c_2+\alpha_{\mathrm{a}})r}\mathrm{d}r\\ &= -4\pi\lambda_{\bar{\mathrm{p}}}c_1(c_2+\alpha_{\mathrm{a}})^{-1}c_3e^{-(c_2+\alpha_{\mathrm{a}})r_{\mathrm{c}}},\end{aligned} \tag{10}$$

and

$$\begin{aligned}\mathcal{L}^{(2)}_{\Delta T}(s)|_{s=0} = &\left(4\pi\lambda_{\bar{\mathrm{p}}}c_1(c_2+\alpha_{\mathrm{a}})^{-1}c_3e^{-(c_2+\alpha_{\mathrm{a}})r_{\mathrm{c}}}\right)^2\\ &+4\pi\lambda_{\bar{\mathrm{p}}}c_1(a_{\mathrm{mn}}c^2_{3,\mathrm{m}} + a_{\mathrm{sd}}c^2_{3,\mathrm{s}})\\ &\cdot\left(r_{\mathrm{c}}^{-1}e^{-(c_2+2\alpha_{\mathrm{a}})r_{\mathrm{c}}} - (c_2+2\alpha_{\mathrm{a}})\mathsf{E}_{\mathsf{i}}((c_2+2\alpha_{\mathrm{a}})r_c)\right),\end{aligned} \tag{11}$$

where $\mathsf{E}_{\mathsf{i}}(x)$ is the exponential integral, i.e., $\mathsf{E}_{\mathsf{i}}(x) = \int_x^\infty t^{-1}e^{-t}\mathrm{d}t$. The mean and variance of $\Delta T$ are as follows.

$$\mathbb{E}[\Delta T] = -\mathcal{L}^{(1)}_{\Delta T}(s)|_{s=0} = 4\pi\lambda_{\bar{\mathrm{p}}}c_1(c_2+\alpha_{\mathrm{a}})^{-1}c_3e^{(c_2+\alpha_{\mathrm{a}})r_{\mathrm{c}}}, \tag{12}$$

$$\begin{aligned}\mathrm{Var}(\Delta T) &= \mathcal{L}^{(2)}_{\Delta T}(s)|_{s=0} - (-\mathcal{L}^{(1)}_{\Delta T}(s)|_{s=0})^2\\ &= 4\pi\lambda_{\bar{\mathrm{p}}}c_1(a_{\mathrm{mn}}c^2_{3,\mathrm{m}} + a_{\mathrm{sd}}c^2_{3,\mathrm{s}})\\ &\cdot\left(r_{\mathrm{c}}^{-1}e^{-(c_2+2\alpha_{\mathrm{a}})r_{\mathrm{c}}} - (c_2+2\alpha_{\mathrm{a}})\mathsf{E}_{\mathsf{i}}(-(c_2+2\alpha_{\mathrm{a}})r_c)\right),\end{aligned} \tag{13}$$

Note that, although moments of a random variable can be directly determined from its Laplace transform, derivation of the distribution of the random variable is not straightforward. In Sec. IV, we present a numerical example in which the distribution of $\Delta T$ is determined based on some approximations.

## IV. Numerical Results

Here, we validate our analytical models through numerical analysis, and explore the effect of different parameters, i.e., NP intensity and transmission power, on the temperature increase of a typical cell. As we have mentioned, the NPs are assumed to be active, i.e., they have energy reserved (for example, from energy harvesting [18]) that enables them to radiate EM waves for communications purposes. Therefore, our numerical results investigate the temperature increase of RBCs induced by active EM radiation from NPs.

TABLE I: List of abbreviated notation

| Parameter | Value |
|---|---|
| Nanoparticle transmit power ($P_{\mathrm{t}}$) | 1 μW |
| EM wavelength | 500 nm |
| Signal duration ($t_{\mathrm{on}}$) | 1 ms |
| Cell intensity ($\lambda_{\mathrm{c}}$) | $5\times10^6$/μl |
| Cell radius ($r_{\mathrm{c}}$) | 2.78 μm |
| Cell specific heat capacity ($\mathsf{c}_{\mathsf{c}}$) | 3.22 J/g/°C |
| Cell mass ($\mathsf{m}_{\mathsf{c}}$) | $101.25\times10^{-12}$ g |
| Cell absorption cross section ($\sigma_{\mathrm{a}}$) [16] | 3.1 μm$^2$ |
| Plasma absorption coefficient ($\alpha_{\mathrm{a}}$) [17] | 0.06 mm$^{-1}$ |
| Plasma specific heat capacity | 3.93 J/g/°C |
| Plasma refractive index | 1.345 |

### A. Simulation Setup

RBCs compose 45% of blood on average [19]. A typical human RBC has a biconcave plate geometry with diameter of approximately $6.2-8.2$ μm and a thickness at the thickest point of $2-2.5$ μm. In this paper, we assume that RBCs form a homogeneous PPP with intensity $\lambda_{\mathrm{c}} = 5\times10^6$ RBCs/μl [19]. For analytical convenience, we approximate the RBCs by spheres [12] with fixed radius $r_{\mathrm{c}} = 2.78$ μm. NPs have the shape of sphere and are also distributed according to a homogeneous PPP. Moreover, we assume that the size of NPs are the same as that of RBCs, i.e., $r_{\mathrm{p}} = r_{\mathrm{c}}$. Therefore, the obstacles that may block EM wave propagation have constant radius $r_{\mathrm{c}}$ with intensity $\lambda_{\mathrm{o}} = \lambda_{\mathrm{c}} + \lambda_{\mathrm{p}}$.

For illustration, we assume that NPs radiate EM waves with a 500 nm wavelength. The antenna pattern has $g_{\mathrm{mn}} = 3$ dB main lobe gain and beamwidth $\psi = 60°$. The parameters $a_{\mathrm{mn}}$, $a_{\mathrm{sd}}$, and side lobe gain $g_{\mathrm{sd}}$ can be determined accordingly from (2). Other parameters are listed in Table I. The RBC mass in Table I is determined assuming an RBC density of 1125 kg/m$^3$. Note that in the simulations, an RBC is heated up if it is exposed to direct EM radiation of an active NP.

### B. Numerical Results

*1) Temperature Increase vs. NP Intensity:* We first validate the mean and variance expressions for the temperature increase derived from the Laplace transform: we compare the mean and variance of $\Delta T$ derived in Sec. III to those obtained from simulations for different NP intensities. The results in Fig. 3(a) and Fig. 3(b) show the mean and standard deviation (STD) of $\Delta T$, respectively. We make three observations about these results. Firstly, we can see that the numerical results from the derived analytical expressions align with the simulation results. Secondly, given the 1 μW transmission power and NP intensities of $50-500$ NP/μl, the average temperature increase over one transmission period is marginal. Thirdly, the mean and STD of $\Delta T$ are almost linear in the NP intensity. On the one hand, the increased NP intensity leads to reduced LOS

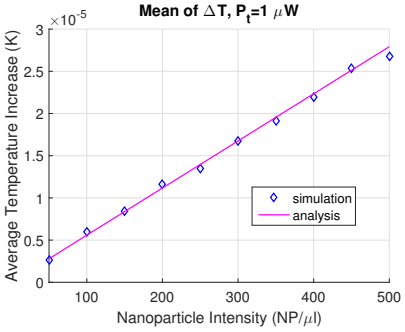


(a) Mean of $\Delta T$

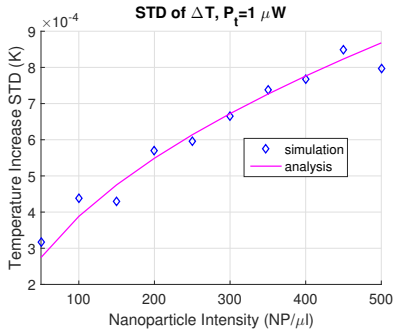


(b) STD of $\Delta T$

Fig. 3: Variation of temperature increase with NP intensities.

probability because the NPs block each other's signals. On the other hand, increasing the NP intensity results in a larger temperature increase according to (12). However, since the NP intensity is very small compared to $\lambda_c$, the mean and STD of $\Delta T$ are still nearly linear in the NP intensity.

*2) Temperature Increase vs. Transmission Power:* The 1 μW ($-30$ dBm) transmission power is determined from the signal duration and the potential energy reservation at an NP [18]. Nevertheless, we also investigate the temperature increase due to different transmission powers that may be configured for an NP. Fig. 4 shows the temperature increase with different transmission powers, from 0.1 μW to 10 μW, with fixed effective NP intensity $\lambda_{\bar{p}} = 50/\mu l$. Note that Fig. 4(c) shows the maximum temperature increase. The analytical approximation of the maximum temperature increase is the temperature increase at the cell that is closest to an NP.

We can observe that the mean, STD, and maximum of $\Delta T$ increase with the transmission power. Note that, the maximum temperature increase is still marginal ($\sim 0.2$ K) even with 10 μW (-20 dBm) transmission power. We can also observe that the maximum temperature increase of the typical cell can be approximated (upper bounded) by the temperature increase at a cell that is closest to an NP. This also means that the severe blockage effect of the dense RBCs prevents an RBC from being heated by a farther NP. This observation provides us some intuition to simply approximate the distribution of $\Delta T$.

### C. Approximating the Distribution of $\Delta T$

According to (9), the Laplace transform of a random variable uniquely determines its moments. In turn, the distribution of the random variable may be found from the moments, e.g., by moment matching [20]. However, as we mentioned previously, the severe blockages prevent the typical cell from being affected by distant NPs. In other words, the temperature increase is largely induced by the nearest NP. It turns out that we can develop a closed-form expression for the distribution of $\Delta T$ with approximations inspired by this insight.

Denote by $d_0$ the distance between the typical cell and the nearest LOS NP. We first derive the cumulative distribution function (CDF) of $d_0$. Note that NLOS NPs can be removed by independent thinning. Let $r$ denote the distance from an NP to the typical cell, the probability that the NP is retained as a LOS NP is $p_L(r)$. Since the NPs with main lobes toward the typical cell contribute significantly more heat, the NPs with side lobes toward the typical cell can be further thinned. Therefore, the average number of LOS NPs with main lobes towards the typical cell within a sphere centered at the typical cell with radius $d$ is

$$\begin{aligned}\Lambda(d,\lambda_{\bar{p}}) &= \int_{|\boldsymbol{x}|<d} p_L(|\boldsymbol{x}|) a_{mn} \lambda_{\bar{p}} (\mathrm{d}\boldsymbol{x}) \\ &= 4\pi a_{mn} \lambda_{\bar{p}} c_1 c_2^{-3} \left(2 - e^{-c_2 d}(c_2^2 d^2 + 2c_2 d + 2)\right).\end{aligned}$$

The CDF of $d_0$ is

$$F_{d_0}(x) = \mathbb{P}(d_0 < x) = 1 - e^{-\Lambda(x,\lambda_{\bar{p}})}. \tag{14}$$

As mentioned, the total temperature increase of the typical cell can be approximated by the temperature increase induced by the nearest NP:

$$\Delta T = \sum_{k \in \Phi_{\bar{p}}} \mathcal{B}_k c_3 \mathcal{G}_k \frac{1}{r_k^2} \approx c_3 g_{mn} \frac{1}{d_0^2}. \tag{15}$$

Therefore, the CDF of $\Delta T$ is

$$\begin{aligned}F_{\Delta T}(x) &= \mathbb{P}(\Delta T < x) = \mathbb{P}(d_0 > \sqrt{c_3 g_{mn}/x}) \\ &= 1 - F_{d_0}(\sqrt{c_3 g_{mn}/x}) = \exp\left(-\Lambda(\sqrt{c_3 g_{mn} x^{-1}}, \lambda_{\bar{p}})\right).\end{aligned}$$

Note that to get a closed-form expression for $F_{\Delta T}(x)$, we also omitted the absorption term, considering the very weak absorption ability of plasma to optical waves, and the very small propagation distance (nearest NP).

Fig. 5 shows the distribution of the temperature increase given $\lambda_{\bar{p}} = 50$ NP/μl and $P_t = 1$ μW. We can see that the analytical expression provides a reasonable approximation to the distribution of $\Delta T$. The curves in Fig. 5 are also justified by the fact that the ratio of NPs to RBCs is very small (50 vs. $5 \times 10^6$ NP/μl), so only a very small number of RBCs get hit directly by NPs' transmissions.

## V. Conclusion

Using stochastic geometry, we investigated the temperature increase of RBCs induced by intra-body optical wireless communications. Specifically, we derived the Laplace transform of temperature increase at a cell, which allowed us to statistically understand the photo-thermal effect induced by EM waves. For the RBC case, we noted that the temperature increase is marginal due to the fact that RBCs actually act as obstacles,

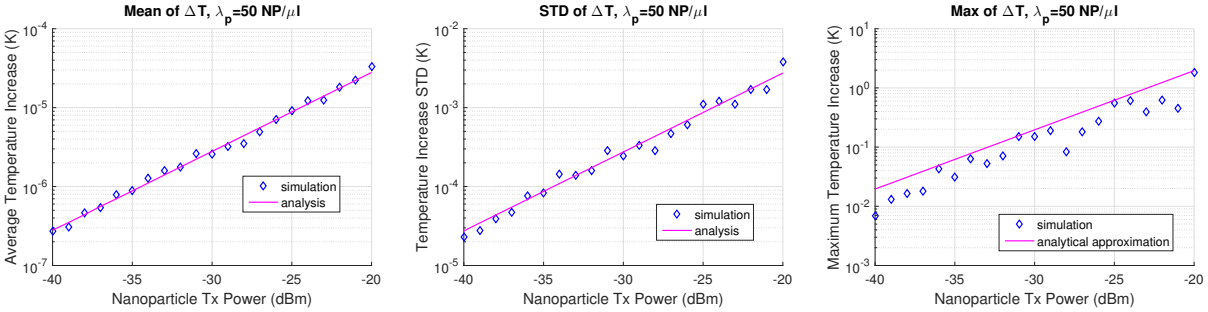


(a) Mean of $\Delta T$ (b) STD of $\Delta T$ (c) Max of $\Delta T$

Fig. 4: Temperature increases induced at different transmission power levels.

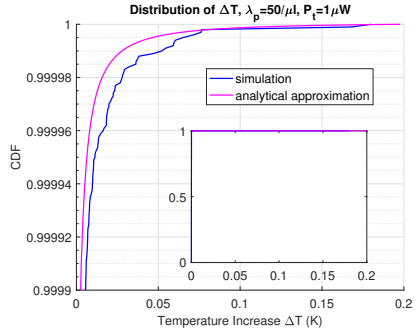


Fig. 5: Distribution of temperature increase. The embedded plot shows the full CDF from $\mathbb{P}(\Delta T < x) = 0$ to $\mathbb{P}(\Delta T < x) = 1$.

which prevent other RBCs from being heated by EM waves, and the very small transmission power of NPs. We also note that the analysis is generic so it is straightforward to apply the framework to other biological tissues. In future work, we will analyze the heat dissipation effect, the evolution of temperature over time, and the $\text{CEM}_{43}$ [5] metric noted in the introduction.

## Appendix A
## Derivation of the Laplace Transform of $\Delta T$

The Laplace transform of the temperature increase is

$$\begin{aligned}
&\mathcal{L}_{\Delta T}(s) \\
&= \mathbb{E}_{\Delta T}\left[e^{-s\Delta T}\right] = \mathbb{E}\left[e^{-sc_3\sum_{k\in\Phi_\text{p}}\mathcal{B}_k\mathcal{G}_k\frac{e^{-\alpha_\text{a} r}}{r_k^2}}\right] \\
&= \mathbb{E}_{\Phi_\text{p},\mathcal{G}_k}\left[\prod_{k\in\Phi_\text{p}}\mathbb{E}_{\mathcal{B}_k}\left[e^{-sc_3\mathcal{B}_k\mathcal{G}_k\frac{e^{-\alpha_\text{a} r}}{r_k^2}}\right]\right] \\
&= e^{-4\pi a_\text{mn}\lambda_\text{p}\int_{r>r_\text{c}}\left(1-\exp\left(-sc_{3,\text{m}}\frac{e^{-\alpha_\text{a} r}}{r^2}\right)\right)p_\text{L}(r)r^2\text{d}r} \\
&\quad\cdot e^{-4\pi a_\text{sd}\lambda_\text{p}\int_{r>r_\text{c}}\left(1-\exp\left(-sc_{3,\text{s}}\frac{e^{-\alpha_\text{a} r}}{r^2}\right)\right)p_\text{L}(r)r^2\text{d}r} \\
&= E_1\cdot e^{4\pi a_\text{mn}\lambda_\text{p}c_1\int_{r>r_\text{c}} r^2e^{-c_2 r}\exp\left(-sc_{3,\text{m}}r^{-2}e^{-\alpha_\text{a} r}\right)\text{d}r} \\
&\quad\cdot e^{4\pi a_\text{sd}\lambda_\text{p}c_1\int_{r>r_\text{c}} r^2e^{-c_2 r}\exp\left(-sc_{3,\text{s}}r^{-2}e^{-\alpha_\text{a} r}\right)\text{d}r} \\
&= E_1 e^{L_\text{mn}(s)+L_\text{sd}(s)},
\end{aligned}$$

where $E_1$, $L_\text{mn}(s)$ and $L_\text{sd}(s)$ are given as in Proposition 1.

## References


[1] M. A. Eckert, P. Q. Vu, K. Zhang, D. Kang, M. M. Ali, C. Xu, and W. Zhao, "Novel molecular and nanosensors for in vivo sensing," *Theranostics*, vol. 3, no. 8, p. 583, 2013.

[2] L. Wu and X. Qu, "Cancer biomarker detection: recent achievements and challenges," *Chemical Soc. Reviews*, vol. 44, no. 10, pp. 2963-2997, 2015.

[3] I. F. Akyildiz and J. M. Jornet, "Electromagnetic wireless nanosensor networks," *Nano Communication Networks*, vol. 1, no. 1, pp. 3-19, 2010.

[4] J. M. Jornet and I. F. Akyildiz, "Channel modeling and capacity analysis for electromagnetic wireless nanonetworks in the terahertz band," *IEEE Trans. Wireless Commun.*, vol. 10, no. 10, pp. 3211-3221, Oct. 2011.

[5] M. W. Dewhirst, et al., "Basic principles of thermal dosimetry and thermal thresholds for tissue damage from hyperthermia," *International Journal of Hyperthermia*, vol. 19, no. 3, pp. 267294, 2003.

[6] H. Elayan, P. Johari, R. M. Shubair, and J. M. Jornet, "Photothermal modeling and analysis of intra-body terahertz nanoscale communication," to appear in *IEEE Trans. NanoBioscience*, 2017.

[7] "COMSOL Multiphysics Simulation Software," COMSOL, [Online], Available: http://www.comsol.com/products/multiphysics/

[8] D. Savéry and G. Cloutier, "A point process approach to assess the frequency dependence of ultrasound backscattering by aggregating red blood cells," *J. Acoust. Soc. Am.*, vol. 110, no. 6, pp. 3252-3262, 2001.

[9] S. Chiu, D. Stoyan, W. Kendall, and J. Mecke, *Stochastic Geometry and Its Applications*, 3rd edition. Wiley, 2013.

[10] F. Baccelli and B. Blaszczyszyn, *Stochastic Geometry and Wireless Networks, Volume I-Theory*. Delft, The Netherlands: NOW, 2009.

[11] H. Guo, P. Johari, J. M. Jornet, and Z. Sun, "Intra-body optical channel modeling for in vivo wireless nanosensor networks," *Trans. NanoBioscience, IEEE*, vol. 15, no. 1, pp. 41-52, Jan. 2016.

[12] P. Johari and J. M. Jornet, "Nanoscale optical channel modeling for in vivo wireless nanosensor networks: a geometrical approach," in *Proc. IEEE ICC*, pp. 1-6, May 2017.

[13] P. Johari and J. M. Jornet, "Nanoscale optical wireless channel model for intra-body communications: Geometrical, time, and frequency domain analyses," *IEEE Transactions on Communications*, 2018.

[14] S. Wu, R. Atat, N. Mastronarde, and L. Liu, "Coverage analysis of d2d relay-assisted millimeter-wave cellular networks," in *Proc. IEEE WCNC*, pp. 1-6, Mar. 2017.

[15] G. Baffou, P. Berto, E. B. Urena, R. Quidant, S. Monneret, J. Polleux, and H. Rigneault, "Photoinduced heating of nanoparticle arrays," *Acs Nano*, vol. 7, no. 8, pp. 6478-6488, 2013.

[16] M. Hammer, *et al.*, "Single scattering by red blood cells," *Applied Optics*, vol. 37, no. 31, pp. 7410-7418, Nov. 1998.

[17] M. Meinke, G. Muller, J. Helfmann, and M. Friebel, "Optical properties of platelets and blood plasma and their influence on the optical behavior of whole blood in the visible to near infrared wavelength range," *Journal of Biomedical Optics*, vol. 12(1), pp. 1-9, Jan./Feb. 2007.

[18] J. M. Jornet and I. F. Akyildiz, "Joint energy harvesting and communication analysis for perpetual wireless nanosensor networks in the terahertz band," *IEEE Trans. Nanotechnology*, vol. 11, no. 3, pp. 570-580, 2012.

[19] "Human blood: composition, blood groups and functions," [Online], Available: http://www.biologydiscussion.com/blood/human-blood-composition-blood-groups-and-functions/52659

[20] C. M. Harris, and W. G. Marchal, "Distribution estimation using laplace transform," *INFORMS J. Computing*, vol. 10 no. 4, Fall 1998.